Article No. jmbi.1999.3350 available online at http://www.idealibrary.com on IDEAL® J. Mol. Biol. (2000) 295, 225–237

JMB

Solution Structure and Backbone Dynamics of the Second PDZ Domain of Postsynaptic Density-95

Hidehito Tochio[1], Franki Hung[1], Ming Li[1], David S. Bredt[2] and Mingjie Zhang[1]*

[1]*Department of Biochemistry The Hong Kong University of Science and Technology, Clear Water Bay, Kowloon, Hong Kong, P. R. China*

[2]*Department of Physiology University of California at San Francisco, San Francisco CA 94143, USA*

**Corresponding author*

The second PDZ domain of postsynaptic density-95 (PSD-95 PDZ2) plays a critical role in coupling *N*-methyl-D-aspartate receptors to neuronal nitric oxide synthase (nNOS). In this work, the solution structure of PSD-95 PDZ2 was determined to high resolution by NMR spectroscopy. The structure of PSD-95 PDZ2 was compared in detail with that of α1-syntrophin PDZ domain, as the PDZ domains share similar target interaction properties. The interaction of the PSD-95 PDZ2 with a carboxyl-terminal peptide derived from a cytoplasmic protein CAPON was studied by NMR titration experiments. Complex formation between PSD-95 PDZ2 and the nNOS PDZ was modelled on the basis of the crystal structure of the α1-syntrophin PDZ/nNOS PDZ dimer. We found that the prolonged loop connecting the βB and βC strands of PSD-95 PDZ2 is likely to play a role in both the binding of the carboxyl-terminal peptide and the nNOS β-finger. Finally, the backbone dynamics of the PSD-95 PDZ2 in the absence of bound peptide were studied using a model-free approach. The ''GLGF''-loop and the loop connecting αB and βF of the protein display some degree of flexibility in solution. The rest of the protein is rigid and lacks detectable slow time-scale (microseconds to milliseconds) motions. In particular, the loop connecting βB and βC loop adopts a well-defined, rigid structure in solution. It appears that the loop adopts a pre-aligned conformation for the PDZ domain to interact with its targets.

Keywords: backbone dynamics; NMR structure; neuronal nitric oxide synthase; PDZ domain; PSD-95

Introduction

Signal transmission in neurons is mediated by a wide variety of ion channels and receptors specifically localized at the synaptic membrane. Rather than freely diffusing in the membrane, these ion channels and receptors form multimeric clusters (for reviews, see Sheng, 1996; Craven & Bredt, 1998; Colledge & Froehner, 1998; O'Brien *et al.*, 1998). Though the molecular mechanisms underlying assembly of the protein networks are largely unknown, recent studies have identified elements critical for synaptic clustering of certain ion channels (Sheng, 1996; Craven & Bredt, 1998; Colledge & Froehner, 1998; O'Brien *et al.*, 1998). For example, clustering of nicotinic acetylcholine receptors at neuromuscular endplates requires a specific 43 kDa protein rapsyn (Apel *et al.*, 1995). More generally, a large class of PDZ (PSD-95, DLG, and ZO-1) domain-containing proteins were identified that mediate targeting and clustering of channels, receptors, cell adhesion proteins, and other signalling enzymes at the specific sites of cell-cell contact, including synapses (Sheng, 1996; Kornau *et al.*, 1997; Craven & Bredt, 1998; Colledge & Froehner, 1998; O'Brien *et al.*, 1998). The membrane-associated guanylate kinase (MAGUK) proteins is a well-studied family of PDZ domain-containing proteins. Mammalian MAGUK proteins include PSD-95/SAP90 (Cho *et al.*, 1992; Kistner *et al.*, 1993), PSD-93/chapsyn-110 (Brenman *et al.*, 1996b; Kim *et al.*, 1996), SAP-97/hdlg (Lue *et al.*, 1994; Müller *et al.*, 1995), and SAP-102 (Müller *et al.*, 1996), all of which are found at synapses (reviewed by Craven & Bredt, 1998). MAGUKs share common domain

Abbreviations used: nNOS, neuronal nitric oxide synthase; PDZ, (PSD-95, DLG and ZO-1); MAGUK, membrane-associated guanylate kinase; GK, guanylate kinase-like; NMDA, *N*-methyl-D-aspartate.

E-mail address of the corresponding author: mzhang@ust.hk

0022-2836/00/020225–13 $35.00/0

organizations consisting of three PDZ domains at the N terminus followed by an SH3 domain. The C-terminal region of MAGUKs encodes a guanylate kinase-like (GK) domain; however, no kinase activity has been detected for the MAGUK proteins. Like the PDZ domains and the SH3 domain, the guanylate kinase domain of MAGUKs functions as a protein-protein interaction module (Naisbitt *et al*., 1997; Brenman *et al*., 1998). The SH3 domain and the GK domain of PSD-95 were found to interact with each other, and such interaction may regulate the protein interaction properties of the modules (McGee & Bredt, 1999).

Much of the current knowledge regarding channel clustering and organizing of the signaling complex by the MAGUK proteins has come from studies of PSD-95. Mutation of PSD-95 in mice leads to an enhanced long-term potentiation and impaired learning (Migaud *et al*., 1998). The protein can multimerize *via* two Cys residues in the N terminus, and the Cys residues play important roles in targeting PSD-95 to cell membrane (Hsueh *et al*., 1997; Craven *et al*., 1999; Hsueh & Sheng, 1999). The first two PDZ domains of PSD-95 can bind specifically to the Shaker K^+ channel or *N*-methyl-D-aspartate (NMDA) receptor NR2 subunits *via* a sequence motif of -E-S/T-X-V* located at the extreme C termini (Kim *et al*., 1995; Kornau *et al*., 1995; Niethammer *et al*., 1996). The second PDZ domain of PSD-95 also binds to the PDZ domain of neuronal nitric oxide synthase (nNOS) (Brenman *et al*., 1996a). Suppression of PSD-95 expression by antisense technology attenuates NO production *via* NMDA receptor-mediated Ca^{2+} influx, suggesting that PSD-95 specifically couples NMDA receptor activation to NO neurotoxicity (Sattler *et al*., 1999). The discovery of the specific coupling between the NMDA receptor and nNOS by the second PDZ domain of PSD-95 makes this PDZ domain an attractive target for designing therapeutic drugs against stroke.

Canonical PDZ domains contain ~80-100 amino acid residues. The PDZ domains form a compact, globular structure consisting of a six-stranded antiparallel β-barrel flanked by two α-helices (Doyle *et al*., 1996; Cabral *et al*., 1996). The carboxyl peptide binds to a groove formed by βB and αB (Doyle *et al*., 1996). Both NMR and X-ray studies showed that the nNOS PDZ domain contains an extra two-strand antiparallel β-sheet C-terminal to the canonical PDZ domain (Tochio *et al*., 1999; Hillier *et al*., 1999). It was proposed that this β-sheet extension is likely to bind to the PDZ2 peptide-binding groove of PSD-95 (Tochio *et al*., 1999). The crystal structure of the nNOS PDZ/α1-syntrophin PDZ dimer indeed showed that the β-sheet extension of the nNOS PDZ binds to the peptide-binding groove formed by βB and αB of α-syntrophin *via* β-invasion (Hillier *et al*., 1999).

In this work, we determined the high-resolution solution structure of the second PDZ domain of PSD-95. The interaction of the PDZ domain with a C-terminal peptide was also investigated. The backbone dynamics of the PDZ domain was studied in detail by ^{15}N-relaxation experiments using a model-free approach.

Results and Discussion

Structural determination

The three-dimensional structure of the second PDZ domain of PSD-95 (referred as PSD-95 PDZ2), that encompasses amino acid residues 155-249 of the native protein was determined in aqueous solution at pH 6.0, 30 °C, using a total of 1835 experimental restraints (Table 1). PSD-95 PDZ2 is a monomeric protein at a concentration up to ~1.5 mM used for NMR studies. The narrow linewidth of the NMR signals and low degree chemical shift degeneration allowed us to obtain a large number of unambiguous NOEs (>18 NOEs per residue). Together with a substantial amount of dihedral and hydrogen bonding restraints, the structure of the protein was determined to a high resolution (Table 1 and Figure 2). The overall backbone precision (root-mean-square deviation, rmsd) of the 20 structural ensembles shown in Figure 2 is 0.31 Å for amino acid residues from 158-246, and 0.29 Å if the flexible βA/βB loop is excluded. The structural statistics are summarized in Table 1. Figure 3 shows a ribbon diagram representation of the PDZ2 structure. The secondary structural elements are labeled following the scheme used by Doyle *et al*. (1996).

The overall structure of PSD-95 PDZ2 is similar to other PDZ domain structures determined by X-ray crystallography and NMR spectroscopy (Doyle *et al*., 1996; Cabral *et al*., 1996; Schultz *et al*., 1998; Daniels *et al*., 1998; Tochio *et al*., 1999; Hillier *et al*., 1999). The protein contains two α-helices (αA and αB) and six β-strands (βA-βF, see Figure 1 for the secondary structure of the protein). The strands of the protein form an antiparallel β-sandwich topology (Figure 3). The 3D structure of PSD-95 PDZ2 is particularly close to that of α1-syntrophin (an rmsd value of 1.36 Å for the entire PDZ domains, Figure 4). The only region that displays significant conformational differences between the PDZ domains of these two proteins is the loop connecting βB and βC (Figure 4). The βB/βC loop of PSD-95 PDZ2 contains an additional six-residue insert when compared to other PDZ domains (Figure 1). A number of long-range NOEs were observed involving the amino acid residues located in the loop turning region (e.g. residues Asn180 and His182) and amino acids at the end of βB and at the beginning of αB. Therefore, the conformation of the βB/βC loop is well defined in solution (Figure 2), and NMR relaxation studies also showed that this loop assumes a rigid conformation (see Figure 8 for more detail). Inspection of the structure of PSD-95 PDZ2 has shown that Asn180 in the βB/βC loop is in close proximity to His225 in the N-terminal end of αB. The His residue at the beginning of αB (His225 in PSD-95

Table 1. Structural statistics for the family of 20 structures

Distance restraints	
Intraresidue ($i - j = 0$)	610
Sequential ($\|i - j\| = 1$)	394
Medium range ($2 < \|i - j\| < 4$)	184
Long range ($\|i - j\| < 5$)	514
Hydrogen bonds	34
Total	1736
Dihedral angle restraints	
Φ	50
Ψ	49
Total	99
Mean r.m.s. deviations from the experimental restraints	
Distance (Å)	0.021 ± 0.001
Dihedral angle (Å)	1.03 ± 0.07
Mean r.m.s. deviations from idealized covalent geometry	
Bond (Å)	0.003 ± 0.000
Angle (Å)	0.46 ± 0.01
Improper (Å)	0.34 ± 0.01
Mean energies (kcal mol^{-1})	
E^{a}_{NOE}	38.5 ± 3.2
E^{a}_{cdih}	6.44 ± 0.88
E_{repel}	50.2 ± 3.4
E_{L-J}	−268.0 ± 9.7
Ramachandran plot[b]	
Residues 158-246	
% residues in the most favorable regions	75.5
additional allowed regions	22.2
generously allowed regions	0.9
Atomic r.m.s. differences (Å)[c]	
Residues 158 to 246 in protein	
Backbone heavy atoms (N, C$^{\alpha}$, and C′)	0.31
Heavy atoms	0.85
Comparison crystal versus solution structures in domain[d]	
R.m.s.d. (Å) N, C$^{\alpha}$, C′atoms	
Secondary structure elements	1.38

None of the structures exhibits distance violations greater than 0.3 Å or dihedral angle violations greater than 5°.

[a] The final values of the square-well NOE and dihedral angle potentials were calculated with force constants of 50 kcal mol^{-1} Å $^{-2}$ and 200 kcal mol^{-1}rad^{-2}, respectively.

[b] The program PROCHECK (Laskowski *et al.*, 1993) was used to assess the overall quality of the structures.

[c] The precision of the atomic coordinates is defined as the average r.m.s. difference between the 20 final structures and the mean coordinates of the protein.

[d] The crystal structure of the third PDZ domain of PSD-95 complexed with a four-residue C-terminal peptide was used for comparison (Doyle *et al.*, 1996).

PDZ2) is known to a play critical role in PDZ domain target recognition specificity through formation of a strong hydrogen bond between N$^{\varepsilon}$ of His and the hydroxyl group of a Ser/Thr residue of an appropriate target (Doyle *et al.*, 1996; Schultz *et al.*, 1998). Residue His182 of PSD-95 PDZ2 occupies a position similar to that of Asn102 of the α1-syntrophin PDZ domain (Figure 1), and Asn102 is directly involved in the binding of the α1-syntrophin PDZ to the ''β-finger'' of nNOS PDZ domain. Chemical shift perturbation studies showed that His182 of PSD-95 PDZ is also involved in binding to a target peptide (see below for more detail). A rigid conformation presumably pre-aligns the amino acid residues of the βB/βC loop to interact with PSD-95 PDZ2 targets, including the nNOS PDZ domain and -S/T-X-V* peptides (see below for more detail).

Target recognition

To understand the molecular basis of C-terminal peptide recognition by PSD-95 PDZ2, we studied the interaction between PDZ2 and a peptide fragment from a recently identified protein called CAPON. Biochemical studies showed that CAPON can competitively dissociate the PDZ/PDZ interaction between nNOS and PSD-95 (Jaffrey *et al.*, 1998). CAPON contains a carboxyl -E-T-A-V* sequence, which matches the PSD-95 PDZ2 recognition motif. Therefore, CAPON may directly bind to PSD-95 in a competitive manner with the nNOS PDZ domain. We used a synthetic peptide comprising the last 12 residues of CAPON (ELGDSLDDETAV) to titrate ^{15}N-labeled PSD-95 PDZ2. Figure 5 summarizes the interaction between PSD-95 PDZ2 and the CAPON peptide using the chemical shift perturbation approach. The data indicate

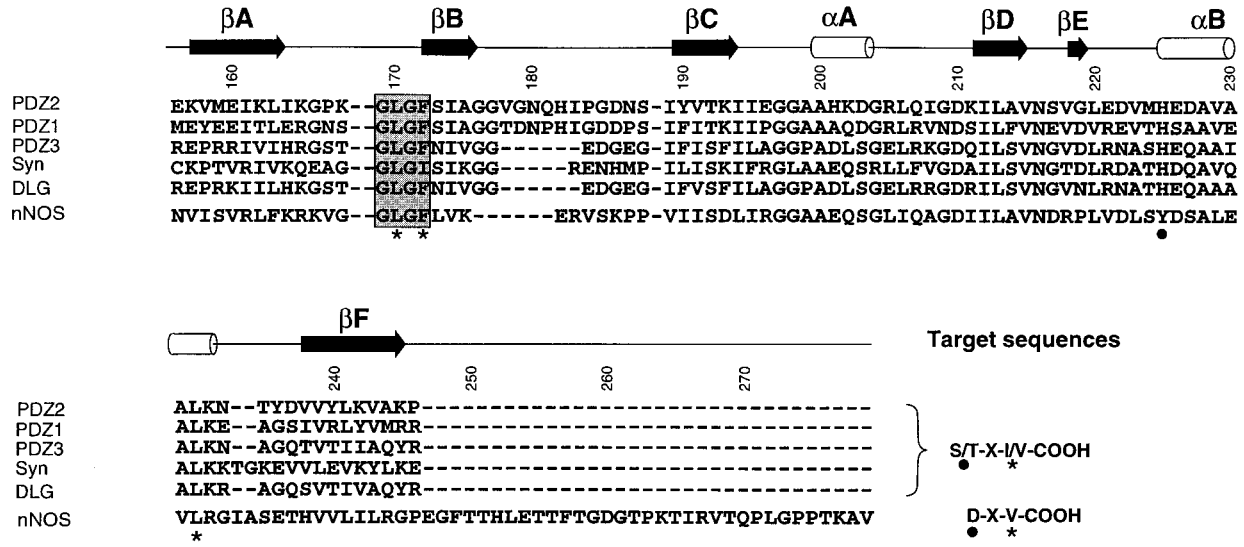

Figure 1. Amino acid sequence alignment of selected PDZ domains. The secondary structure of PSD-95 PDZ2 determined from this work is included at the top of the sequences. The GLGF motif is highlighted with a shaded box. The amino acid residues forming the hydrophobic pocket, which accommodate the side-chain of the amino acid residue at the 0 position of carboxyl peptides, are labeled with asterisks (*). The αB2 amino acid residue that plays a critical role in selecting the residue at the −2 position of peptides is indicated with a black dot. The target peptide sequences for the PDZ domains are included.

that the CAPON peptide can indeed bind to the expected peptide-binding groove located between αB and βB. The peptide-binding-induced conformational changes are particularly obvious in the GLGF loop and the αB/βF loop of PSD-95 PDZ2. It is noteworthy that His182, located at the tip of the βB/βC loop, also undergoes a large chemical shift change upon binding to the CAPON peptide, indicating that the well-defined βB/βC loop is directly involved in target peptide binding (Figure 5). The data in Figure 5 also substantiate that PDZ domains undergo localized conformational changes only upon binding to their targets (Doyle *et al.*, 1996; Hillier *et al.*, 1999; Tochio *et al.*, 1999). To assess whether the C-terminal 12 residues of CAPON is sufficient for PSD-95 PDZ2 binding, we have used a C-terminal 125 residue fragment of CAPON to titrate ^{15}N-labeled PSD-95 PDZ2. A chemical shift perturbation profile essentially identical with that shown in Figure 5 was obtained, indicating that only the short carboxyl end of CAPON is involved in binding to PSD-95 PDZ2.

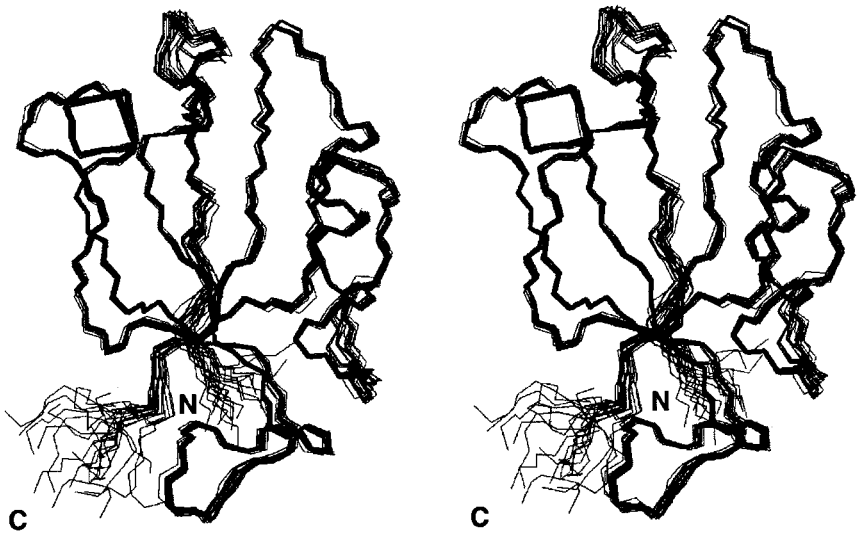

Figure 2. Stereoview showing the best-fit superposition of the backbone atoms (N, C^{α}, and C′) of the final 20 structures of PSD-95 PDZ2. The structures are superimposed against the average structure using the residues 158-246. The program MOLMOL (Koradi *et al.*, 1996) was used to generate the Figure.

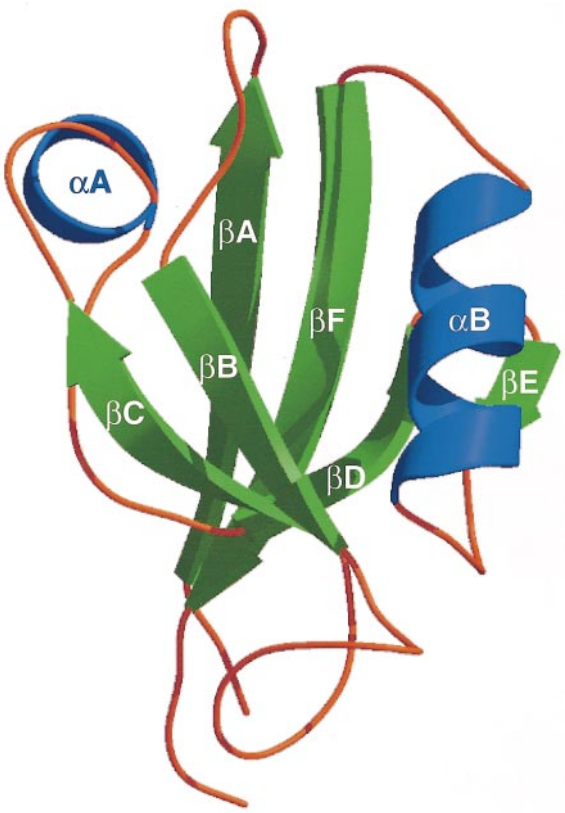

Figure 3. Ribbon diagram presentation of PSD-95 PDZ2. The secondary structure elements are labeled following the scheme used in the crystal structure of PSD-95 PDZ3 (Doyle *et al.*, 1996). The Figure was generated using MOLSCRIPT (Kraulis, 1991) and Raster3D (Merritt & Murphy, 1994).

The selection mechanism of a Val and a Ser/Thr residue at 0 and −2 positions, respectively, of carboxyl peptides by the PSD-95 PDZ domains has been clearly demonstrated in the PDZ/peptide complex structures previously determined (Doyle *et al.*, 1996; Schultz *et al.*, 1998; Tochio *et al.*, 1999). Orientated peptide library studies further showed that PDZ domains display some degree of selectivity at the −1 position of the carboxyl peptides. For example, a negatively charged residue (Asp/Glu) at this position is strongly preferred by PSD-95 PDZ1 and PDZ2; whereas the PDZ3 domain of the protein selects a Ser/Thr residue at the corresponding position (Songyang *et al.*, 1997; Niethammer *et al.*, 1998). The selectivity for the −1 position of carboxyl peptides is largely determined by the second amino acid residue in the βB of the PDZ domains, as the side-chains of the βB2 residue and the amino acid residue in the −1 position of the carboxyl peptides are in close proximity. In PSD-95 PDZ1 and PDZ2, a Ser residue in βB2 could form a hydrogen bond with the carboxyl group of Asp/Glu of carboxyl peptides, presumably explaining the selection of a negatively charged Asp/Glu at the −1 position of the peptide (Figure 1). Mutation of βB2 Asn to a Ser residue switches the binding specificity of PSD-95 PDZ3 to one that selects a carboxyl peptide possessing Asp/Glu at the −1 position (Niethammer *et al.*, 1998). The βB2 residue of the nNOS PDZ is the hydrophobic amino acid Leu, and thus the nNOS PDZ domain selects hydrophobic amino acid residues such as Leu, Pro, and Ala at the −1 position of the peptides (Stricker *et al.*, 1997; Schepens *et al.*, 1997). The first PDZ domain of Mint1 contains Val in the βB2 position, and thus it selects bulky hydrophobic amino acid residues such as Trp at the −1 position of carboxyl peptides (Maximov *et al.*, 1999). The PDZ domains of actinin-associated, LIM domain-containing proteins ALP, Cypher, and Enigma contain Arg at the βB2 position, and these PDZ domains select a negatively charged Asp/Glu at the −1 position of the target peptides (Xia *et al.*, 1997; Zhou *et al.*, 1999; D.S.B., unpublished results). However, we note that the selection of the −1 position amino acid residue of the target peptide by PDZ domains is not a strict requirement, as a number of PDZ domains do not display the selection mechanism discussed above. It is possible that other regions of the PDZ domain may contribute to the amino acid residue selection at the −1 position of the target peptides.

In addition to binding carboxyl-terminal peptides, PSD-95 PDZ2 can specifically bind to an internal peptide fragment from nNOS (Brenman *et al.*, 1996a). As shown in Figure 4, the 3D structures of PSD-95 PDZ2 and the α1-syntrophin PDZ are remarkably similar. Both PDZ domains are capable of binding to the nNOS PDZ domain (Brenman *et al.*, 1995, 1996a). We therefore modeled a PSD-95 PDZ2 and the nNOS PDZ dimer complex based on the structure of the α1-syntrophin PDZ/nNOS PDZ dimer (Hillier *et al.*, 1999). Figure 6 shows the model of the PSD-95 PDZ2/nNOS PDZ dimer. By simply superimposing the PDZ domains of PSD-95 and α1-syntrophin, the ''β-finger'' of the nNOS PDZ fits snugly into the peptide-binding groove of PSD-95 PDZ2. Deletion of the β-finger of nNOS completely abolished its interaction with PSD-95 PDZ2 (H.T. & M.Z., unpublished results). In addition to the expected contacts between the β-finger of nNOS PDZ and βB, αB as well as the GLGF-loop of PSD-95 PDZ2, the βB/βC loop of PSD-95 PDZ2 is in close proximity to the β-finger of the nNOS PDZ (Figure 6).

^{15}N T_1, T_2, and NOE data

^{15}N T_1, T_2, and NOE values of 76 out of 95 residues were obtained (Figure 7(a)-(c)). Of the 19 uncharacterized residues, Leu170 and Ser217 were too weak to obtain reliable experimental data, Pro167, Pro184, and Pro246 do not contain amide protons, and the remaining residues were overlapped in the 2D ^{1}H-^{15}N HSQC spectrum of PSD-95 PDZ2. The average values are (the residues with ^{1}H-^{15}N NOE values less than 0.6 are trimmed) 0.44(±0.02) second, 0.13(±0.01) second, 0.74(±0.05)

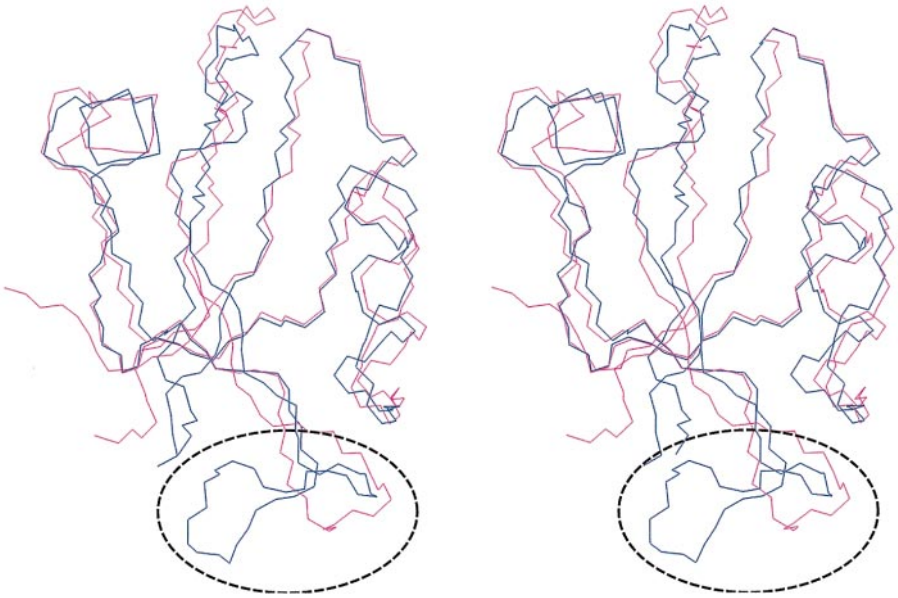

Figure 4. Comparison of the 3D structures of PSD-95 PDZ2 and the α1-syntrophin PDZ domain. The backbone traces (N, C^{α}, and C′) of PSD-95 PDZ2 (blue) and the α1-syntrophin PDZ domain (red) are superimposed. The two structures were fitted to each other by excluding the GLGF-loop, βB/βC loop and the two termini. The rmsd between the backbones of the two PDZ domains is 1.36 Å. The loops connecting the βB and βC strands in both structures are highlighted with a dotted oval.

and 3.50(±0.18) for T_1, T_2, NOE, and T_1/T_2, respectively. The mean T_1/T_2 value was initially used to estimate the overall correlation time (τ_m) of the protein, and a mean τ_m value of 5.98(±0.21) ns was obtained. In this calculation, residues with T_1/T_2 values one standard deviation smaller/larger than the mean value were excluded on the grounds that these residues may undergo conformational exchange or are better modeled using two-time-scale spectral density function (Farrow *et al.*, 1994). The global τ_m value was also obtained, while S^2 and τ_e were optimized for individual residues. The global τ_m value was determined to be 6.04 ns. The mean τ_m value obtained from the T_1/T_2 ratios agrees very well with the global τ_m value.

Backbone dynamics of PSD-95 PDZ2

The T_1, T_2, and NOE values, and the τ_m value, estimated from the average T_1/T_2 value, were used to fit to the extended Lipari-Szabo dynamic models following the methodology described by Mandel *et al.* (1995). Five models were considered, which included: (1) S^2 only, τ_e and R_{ex} are negligible; (2) S^2 and τ_e only, R_{ex} is negligible; (3) S^2 and an R_{ex} term; (4) S^2, τ_e, and R_{ex}; and (5) incorporation of an additional order parameter for two-time-scale internal motions (S_f^2 and S_s^2 for internal motions on the fast and slow time-scales). Figure 8(a) and (b) show the fitted S^2 and τ_e values of PSD-95 PDZ2. Only two residues of PSD-95 PDZ2 (Gly171 and Ile174) need R_{ex} to fit T_1, T_2, and NOE values, and the R_{ex} values are both below 1.0 s^{-1} (hence the R_{ex} values are not plotted). The result indicates that PSD-95 PDZ2 lacks slow time-scale chemical motions of the order of microseconds to milliseconds. Analysis of the relaxation data by including anisotropic tumbling did not yield better fitting data compared to those shown in Figure 8 (data not shown), suggesting that the overall anisotropic motion of the protein is negligible. In addition, the reproducible line-width of the ^1H-^{15}N HSQC spectrum of the protein throughout the experiments ruled out the possibility of protein aggregation.

In general, the amino acid residues in the secondary structure regions have order parameter (S^2) values of ~0.9, and the relaxation data of these residues can be fitted by model 1 (Figure 8). The result indicates that the secondary structure regions of the protein behave rigidly in solution on the picosecond to nanosecond time-scale (Figure 8(a)). The lack of R_{ex} terms for these residues further indicates that the α-helices and β-strands of the protein lack concerted motion on a microsecond to millisecond time-scale. As expected, the residues at both termini of the protein have lower S^2 values, and these residues require τ_e to model the relaxation data due to the fast internal motions. The loops connecting βA/βB and αB/βF also have somewhat lower S^2 values, and experience fast internal motions in addition to the nanosecond time-scale tumbling of the entire protein, indicating that both loops undergo mild hinge motion in solution (Figure 8). The data in Figure 2 also showed that both of the loops display some degree of coordinate dispersion. The βA/βB and αB/βF loops are directly involved with the binding of the target peptide, as shown by the

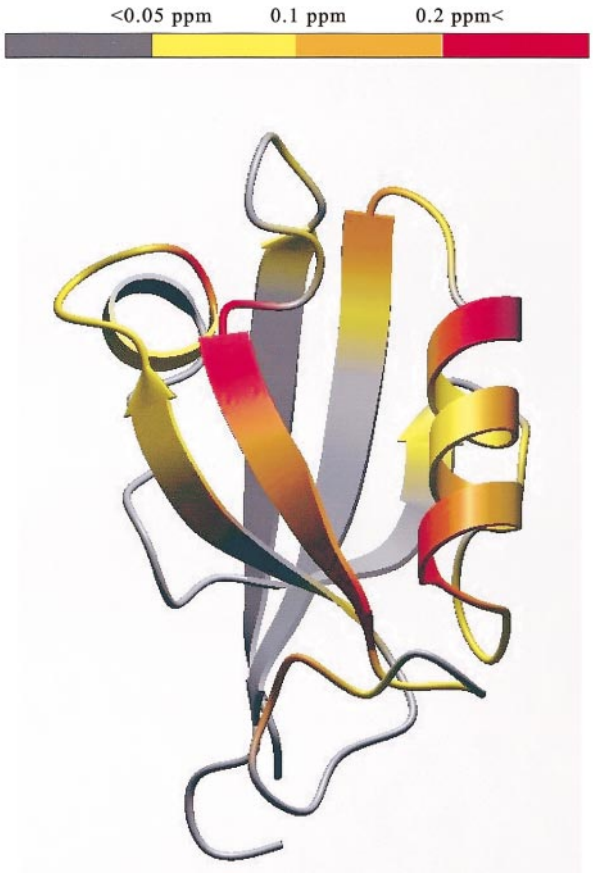

Figure 5. Chemical shift changes of PSD-95 PDZ2 resulted from the CAPON peptide binding. The combined ^{1}H and ^{15}N chemical shift changes are defined as:

$$\Delta_{ppm} = \sqrt{(\Delta\delta_{HN})^2 + (\Delta\delta_N * \alpha_N)^2}$$

The scaling factor (α_N) used to normalize the ^{1}H and ^{15}N chemical shifts is 0.17. The assignment of the CAPON peptide bound form of PSD-95 PDZ2 was obtained by stepwise titration of the ^{15}N-labeled protein with the peptide. The coloring scheme is presented using a horizontal bar at the top. The Figure was prepared using the program MOLMOL.

chemical shift perturbation studies (Figure 5). The βA/βB loop contains the GLGF-motif of the protein, and the backbones of the residues in this region are expected to form hydrogen-bonding interactions with the carboxyl group of the amino acid residue at the 0 position of target peptides. The residues in the αB/βF loop form hydrophobic contacts with the side-chain of the residue at the 0 position of target peptide. Both loops are expected to undergo significant conformational changes after binding to the peptides. The loop connecting βE and αB is also flexible in free PSD-95 PDZ2, and is expected to remain flexible after binding to the target peptide, as little chemical shift changes were observed in this loop upon binding to the CAPON peptide. The PSD-95 PDZ2 contains two rigid loops with significant lengths, one of which is the eight residue loop connecting αA and βD, and the other a 13 residue loop connecting βB and βC strands. The amino acid residues in the αA/βD loop intimately interact with residues from βC, forming the core of the protein, even though the loop does not adopt a regular secondary structure. Therefore, the loop has rigidity similar to the secondary structure regions of the protein. The residues in the βB/βC loop of PSD-95 PDZ2 are also fairly rigid, although the order parameters of the loop are somewhat lower than the secondary structure regions (S^2 values of ~0.8). Additionally, the relaxation data of the loop require τ_e to be modeled, indicating that the entire loop undergoes cooperative fast time-scale fluctuation. NOE data also indicated that the entire βB/βC loop is well defined in solution (Figure 2). A chemical shift perturbation study showed that some residues in the loop experience large chemical shift changes upon binding to the CAPON peptide (Figure 5). The interaction model between PSD-95 and the nNOS PDZ also suggests that the βB/βC loop directly contacts the β-finger of the nNOS PDZ domain (Figure 6). Indeed, we also observed large chemical shift changes of a number of amino acid residues in the βB/βC loop when PSD-95 PDZ2 binds to the nNOS PDZ domain (H.T. & M.Z., unpublished results). It is likely that the βB/βC loop of PSD-95 is pre-aligned in a conformation for interacting with its targets. A majority of the PDZ domains have much shorter βB/βC loops, and the loop is generally not directly involved in binding to target peptides (Doyle *et al.*, 1996; Tochio *et al.*, 1999). The extra insert of six or seven residues in the βB/βC loop may play some role in determining the target-binding specificity of PSD-95 PDZ2. In particular, the βB/βC loop may be essential for PSD-95 PDZ2 to interact with an internal peptide such as the β-finger of nNOS. However, experimental evidence is required to substantiate the above hypothesis.

Summary

The solution structure of PSD-95 PDZ2 has been determined to a high resolution. The overall structure of the PSD-95 PDZ2 is similar to that of other known PDZ domains. The PSD-95 PDZ2 contains a long, rigid loop connecting the βB and βC strands, and this unique loop is directly involved in target binding. The elucidation of the high-resolution structure lays essential groundwork in understanding the molecular mechanism of PSD-95 PDZ2 in recognizing both C-terminal peptides and internal peptide fragments. In addition, the 3D structure determined in this work will be invaluable in designing small molecular mass compounds aimed at blocking nNOS binding to PSD-95. Such compounds may act as potential drug leads against stroke with high specificity. Relaxation studies showed that the PSD-95 PDZ2 is, overall, a rigid molecule. The peptide-binding groove is also rigid, with the exception of the

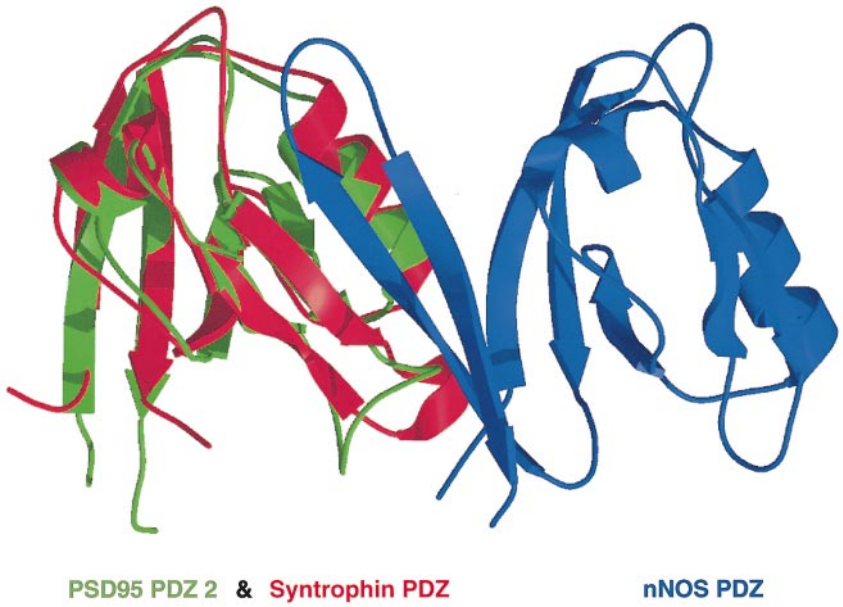

Figure 6. Model of the PSD-95 PDZ2 and the nNOS PDZ complex. In this model, PSD-95 PDZ2 (green) is superimposed on the α1-syntrophin PDZ domain (red) (Hillier *et al.*, 1999). The nNOS PDZ domain is shown in blue. The Figure was generated using MOLSCRIPT and Raster3D.

GLGF-motif-containing loop and the αB/βF loop, which display mild flexibility in the absence of its targets. It is likely that formation of the PSD-95 PDZ2 and peptide complex is supported by the flexibility in the target peptide rather than the PDZ domain.

Materials and Methods

Cloning, expression, and purification of PSD-95 PDZ2

The second PDZ domain of rat PSD-95 encompassing amino acid residues 155-249 of the protein was PCR amplified from the full-length PSD-95 gene using the following two primers: 5′-CTGCTCGAGGCCGAAAAGGTC-3′ (coding strand) and 5′-CTGGATCCTAGGCATTGCTG-3′ (non-coding strand). The amplified PSD-95 PDZ2 fragment was inserted into the *Xho*I and *Bam*HI sites of the plasmid pET14b (Novagen). The pET14b plasmid harboring the PSD-95 PDZ2 gene was then transformed into *Escherichia coli* BL21(DE3) host cells. To express the protein, the host cells containing the PSD-95 PDZ2 plasmid were grown in LB medium at 37 °C until the A_{600} reached ~1.0. The expression of the protein was induced by the addition of IPTG to a final concentration of 0.5 mM. The culture was incubated for three hours at the same temperature after the addition of IPTG. Uniformly ^{15}N and $^{15}N/^{13}C$-labeled PDZ2 were prepared by growing the bacteria in M9 minimal medium using $^{15}NH_4Cl$ (1 g/liter) as the sole nitrogen source or $^{15}NH_4Cl$ (1 g/liter) and $^{13}C_6$-labeled glucose (1 g/liter) as the sole nitrogen and carbon source, respectively.

Recombinant PSD-95 PDZ2 was purified by conventional chromatographic techniques. Cell pellets from 2 l of bacterial cultures were first resuspended in 20-30 ml of Ni^{2+}-NTA affinity column buffer (20 mM Tris-HCl (pH 7.9), 5 mM imidazole, 0.5 M NaCl) containing 1 mM PMSF, 1 μg/ml leupeptin, and 1 μg/ml of antipain. Cells were lysed by three passes through a French press, and the viscosity of the suspension was reduced by sonication. The cell lysate was centrifuged at 30,000 *g* for 30 minutes, and the supernatant was loaded onto a Ni^{2+}-NTA column. The His-tagged PSD-95 PDZ2 was eluted from the Ni^{2+}-NTA column following the instructions of the manufacturer (Novagen). The N-terminal His-tag was cleaved by digesting His-PDZ2 eluted from the Ni^{2+}-NTA column with thrombin (one unit of enzyme per mg of His-PDZ2 for two hours at room temperature). The His-tag and small amounts of contaminants were removed from PSD-95 PDZ2 by passing the digestion mixture through a Sephacryl-100 gel-filtration column (Amersham Pharmacia Biotech). The purified PSD-95 PDZ2 was extensively dialyzed against 10 mM NH_4CO_3 buffer, freeze-dried, and stored at −80 °C.

NMR experiments

Four NMR samples were prepared for structural determination of the PSD-95 PDZ2 with a protein concentration of ~1.5 mM (unlabeled PDZ2 in 99.9 % ^2H_2O, ^{15}N-labeled protein in 90 % H_2O/10 % ^2H_2O, two $^{15}N/^{13}C$-labeled samples in 99.9 % ^2H_2O and in 90 % H_2O/10 % ^2H_2O). The protein was dissolved in 100 mM potassium phosphate buffer at pH 6.0 (direct meter reading). A freshly prepared ^{15}N-labeled sample in 90 % H_2O/10 % ^2H_2O (~ 1.0 mM) was used for relaxation data measurements.

All NMR experiments were carried out at 30 °C on Varian Inova 500 and 750 spectrometers equipped with 5 mm *z*-shielded gradient triple resonance probes. NMR spectra were processed with nmrPipe software package (Delaglio *et al.*, 1995) and analyzed using PIPP (Garrett *et al.*, 1991). Sequential backbone resonance assignments of the protein were obtained by standard heteronuclear correlation experiments including HNCO, HNCACB, CBCA(CO)NH, H(CCO)NH, and C(CO)NH experiments, and confirmed by a 3D ^{15}N-separated NOESY experiment (Bax & Grzesiek, 1993; Kay & Gardner, 1997). The non-aromatic, non-exchangeable side-chain assignments were obtained using an HCCH-TOCSY experiment. The side-chains of aromatics were assigned by ^1H 2D TOCSY and NOESY experiments of an unlabeled protein sample in ^2H_2O. The side-chains -NH_2 of Asn and Gln residues

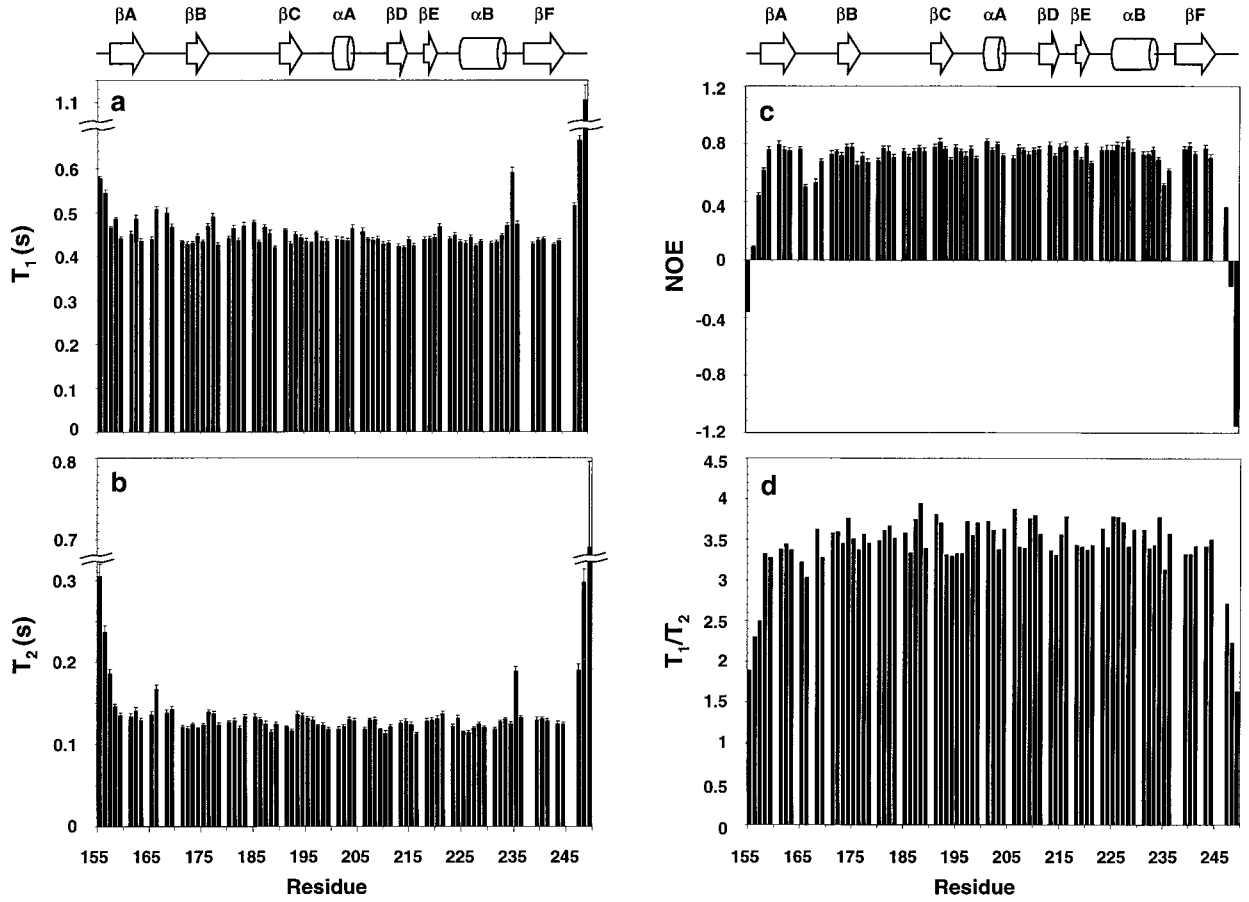

Figure 7. Plot as a function of amino acid residue number of measured (a) T_1, (b) T_2, (c) ^{1}H-^{15}N NOE, and (d) calculated T_1/T_2 ratios of PSD-95 PDZ2. The experimental errors in measuring T_1, T_2, and ^{1}H-^{15}N NOE values are included. The secondary structure of the protein is included at the top.

were assigned by a 3D ^{15}N-separated NOESY experiment of the ^{15}N-labeled protein dissolved in H_2O.

The pulse sequences used to obtain ^{15}N longitudinal relaxation times, T_1, the ^{15}N spin-lattice relaxation times, T_2, and ^{1}H-^{15}N steady-state NOE values were as described (Farrow *et al.*, 1994). ^{15}N, T_1, T_2 and ^{1}H-^{15}N NOE measurements were performed at 30 °C on the Varian Inova 500-MHz spectrometer. The relaxation delays T for T_1 experiments were: $T = 0.01$, 0.08, 0.18, 0.30, 0.45, 0.64, 0.90, 1.30 seconds, and T for T_2 were: $T = 0.014$, 0.029, 0.043, 0.058, 0.072, 0.086, 0.100, 0.130 second. Steady-state ^{1}H-^{15}N NOE values were determined at 500 MHz by recording spectra with and without a three second ^{1}H saturation prior to the start of the experiment. The total recycle delays for the NOE measurement with and without ^{1}H saturation were four and seven seconds, respectively. The recycle delays for ^{15}N T_1 and T_2 measurements were two seconds. A total of 16 transients were collected in T_1 and T_2 experiments, and 24 scans were acquired in NOE measurements. All of the spectra were recorded as 128 × 512 complex data matrices. Lorentzian-to-Gaussian apodization functions were applied in both dimensions before Fourier transformation. All data were processed using nmrPipe software (Delaglio *et al.*, 1995), and peak intensities were characterized as volumes using surface fitting routines in the nmrPipe software.

The steady-state NOE values were determined from the ratios of the peak volumes with and without proton saturation:

$$\mathrm{NOE} = I_{\mathrm{sat}}/I_{\mathrm{unsat}} \tag{1}$$

T_1 and T_2 values were determined by fitting the measured peak volumes to a two-parameter function of:

$$I(t) = I_0 \exp(-t/T_{1,2}) \tag{2}$$

where $I(t)$ is the peak volume after a delay of time t and I_0 is the volume at time $t = 0$. A conjugate gradient minimization was performed to determine the optimum value of the I_0 and $T_{1,2}$ parameters by minimizing the goodness of fitting (χ^2):

$$\chi^2 = \Sigma(I_c(t) - I_e(t))^2/\sigma I^2 \tag{3}$$

where $I_c(t)$ and $I_e(t)$ are the intensities from the fitting and experimental measurement, respectively, σI is the standard deviation of the experimental intensity measurements.

The spectral density function can be modeled using a model-free formalism (Lipari & Szabo, 1982a,b), assuming that a molecule tumbles isotropically, and the timescales for the internal motions approach the extreme narrowing regime:

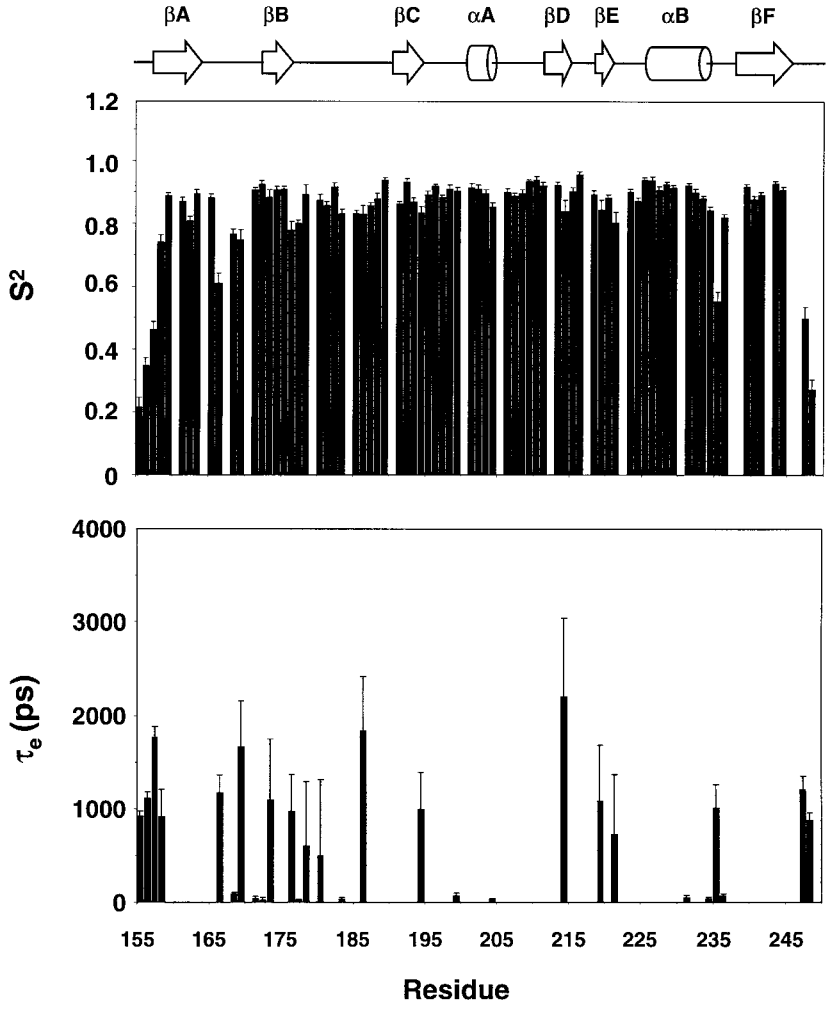

Figure 8. Results from the model-free analysis are plotted as a function of amino acid sequence. Only (a) S^2 and (b) τ_e are sufficient to describe the backbone dynamics of PSD-95 PDZ2. The τ_e values derived from model 5 represent τ_s in equation (5).

$$J(\omega) = S^2\tau_m/(1+\omega^2\tau_m^2) + (1-S^2)\tau/(1+\omega^2\tau^2) \quad (4)$$

where $J(\omega)$ is the spectral density function, the order parameter S^2 describes the degree of spatial restriction of the internal motion of a ^1H-^{15}N bond vector, τ_m is the overall correlation time of a molecule. The effective correlation time resulting from the internal motions is described by τ_e, where $1/\tau = 1/\tau_m + 1/\tau_e$. An extended form of the model-free spectral density function was used (Clore *et al.*, 1990) to incorporate parameters for internal motional processes on two distinct time-scales, differing by at least an order of magnitude:

$$J(\omega) = S^2\tau_m/(1+\omega^2\tau_m^2) + (S_f^2 - S^2)\tau/(1+\omega^2\tau^2) \quad (5)$$

where $S^2 = S_f^2 S_S^2$, S_f^2 and S_S^2 are the squares of the order parameters for the internal motions on the fast and slow time-scales, respectively. The effective correlation time for the slow internal motions, τ_s, is included using relationship $1/\tau = 1/\tau_m + 1/\tau_s$.

An additional term, R_{ex}, is required when modeling experimental T_2 values to account for the contributions from processes other than those from dipole-dipole and chemical shift anisotropy:

$$1/T_2 = 1/T_{2(DD)} + 1/T_{2(CSA)} + R_{ex} \quad (6)$$

where $1/T_{2(DD)}$ and $1/T_{2(CSA)}$ are contributions of dipole-dipole and chemical shift anisotropy to transverse relaxation, and R_{ex} is in most cases the contribution of conformational averaging of a molecule.

The selection of the most appropriate spectral density function for modeling the relaxation parameters of each residue was based on the following equation:

$$\chi^2 = (T_{1c} - T_{1e})^2/\sigma T_1^2 + (T_{2c} - T_{2e})^2/\sigma T_2^2 + (\mathrm{NOE_c} - \mathrm{NOE_e})^2/\sigma\mathrm{NOE}^2 \quad (7)$$

where the subscripts c and e represent calculated and experimentally measured relaxation parameters, respectively, and σT_1, σT_2, and σNOE are estimates of the standard deviation of the experimentally determined parameters. Non-linear least-squares optimization and Monte Carlo error analysis were performed for the variables in each of the following spectral density functions: (1) a function of the form given in equation (4) with τ_e fixed at zero; (2) the same function with τ_e used as a fitting parameter; (3), the functional form described in equation (4) with τ_e fixed at zero but including the term R_{ex} to account for conformational exchange; (4) the functional form in equation (4), including both τ_e and R_{ex} as fitting parameters; and (5) finally the two-time-scale form of the spectral density function given in equation (5). The relaxation data were fit using the program Modelfree 4.0 (provided by A.G. Palmer). The selection

criteria of the dynamic models followed those described earlier (Mandel *et al*., 1995).

Structural calculations

Approximate interproton distance restrains were derived from three NOESY spectra (a ^{1}H 2D homonuclear NOESY, a ^{15}N-separated-NOESY, and a ^{13}C-separated NOESY). NOEs were grouped into three distance ranges 1.8-2.7 Å (1.8-2.9 Å for NOEs involving NH protons), 1.8-3.3 Å (1.8-3.5 Å for NOEs involving NH protons), and 1.8-5.0 Å, corresponding to strong, medium, and weak NOEs. Hydrogen bonding restraints (two per hydrogen bond where $r_{\text{NH-O}} = 1.8\text{-}2.2$ Å and $r_{\text{N-O}} = 2.2\text{-}3.3$ Å) were generated from the standard secondary structure of the protein based on the NOE patterns, and backbone secondary chemical shifts (Tochio *et al*., 1998). Backbone dihedral angle restraints (ϕ and ψ angles) were derived from $^{3}J_{\text{HN}\alpha}$ coupling constants measured using an HMQC-*J* experiment and backbone chemical shift analysis program TALOS (Cornilescu *et al*., 1999). Structures were calculated using a torsion angle dynamics/simulated annealing protocol (Nilges *et al*., 1988; Stein *et al*., 1997) using the program X-PLOR 3.8 (Brünger, 1992).

Coordinates

The coordinates of the structures of PSD-95 PDZ2 have been deposited in the Protein Data Bank, accession code 1qlc.

Acknowledgments

We thank L. E. Kay for providing NMR pulse sequences, A. G. Palmer for the program Modelfree 4.0 for relaxation data analysis, S. R. Jaffrey for the CAPON clone, Dr M. Nilges for the help in torsion angle dynamic calculations of the NMR structures, and D. Miller-Martini for critical reading and comments on the manuscript. This work is partially supported by grants from the Research Grant Council of Hong Kong to M.Z. (HKUST6189/97 M, 6198/99 M). The NMR spectrometers used in this work were purchased by the Biotechnology Research Institute of HKUST.

References

Apel, E. D., Roberds, S. L., Campbell, K. P. & Merlie, J. P. (1995). Rapsyn may function as a link between the acetylcholine receptor and the agrin-binding dystrophin-associated glycoprotein complex. *Neuron,* **15**, 115-126.

Bax, A. & Grzesiek, S. (1993). Methodological advances in protein NMR. *Acc. Chem. Res.,* **26**, 131-138.

Brenman, J. E., Chao, D. S., Xia, H., Aldape, K. & Bredt, D. S. (1995). Nitric oxide synthase complexed with dystrophin and absent from skeletal muscle sarcolemma in Duchenne muscular dystrophy. *Cell,* **82**, 743-752.

Brenman, J. E., Chao, D. S., Gee, S. H., McGee, A. W., Craven, S. E., Santillano, D. R., Wu, Z., Huang, F., Xia, H., Peters, M. F., Froehner, S. C. & Bredt, D. S. (1996a). Interaction of nitric oxide synthase with the postsynaptic density protein PSD-95 and alpha1-syntrophin mediated by PDZ domains. *Cell,* **84**, 757-767.

Brenman, J. E., Christopherson, K. S., Craven, S. E., McGee, A. W. & Bredt, D. S. (1996b). Cloning and characterization of postsynaptic density 93, a nitric oxide synthase interacting protein. *J. Neurosci.* **16**, 7407-7415.

Brenman, J. E., Topinka, J. R., Cooper, E. C., McGee, A. W., Rosen, J., Milroy, T., Ralston, H. J. & Bredt, D. S. (1998). Localization of postsynaptic density-93 to dendritic microtubules and interaction with microtubule-associated protein 1A. *J. Neurosci.* **18**, 8805-8813.

Brünger, A. T. (1992). *X-PLOR. A System for X-ray Crystallography and NMR*, Yale University Press, New Haven, CT.

Cabral, J. H., Petosa, C., Sutcliffe, M. J., Raza, S., Byron, O., Poy, F., Marfatia, S. M., Chishti, A. H. & Liddington, R. C. (1996). Crystal structure of a PDZ domain. *Nature,* **382**, 649-652.

Cho, K.-O., Hunt, C. A. & Kennedy, M. B. (1992). The rat brain postsynaptic density fraction contains a homolog of the *Drosophila* discs-large tumor suppressor protein. *Neuron,* **9**, 929-942.

Clore, G. M., Szabo, A., Bax, A., Kay, L. E., Driscoll, P. C. & Gronenborn, A. M. (1990). Deviations from the simple two-parameter model-free approach to the interpretation of nitrogen-15 nuclear relaxation of proteins. *J. Am. Chem. Soc.* **112**, 4989-4991.

Colledge, M. & Froehner, S. C. (1998). Signals mediating ion channel clustering at the neuromuscular junction. *Curr. Opin. Neurobiol.* **8**, 357-363.

Cornilescu, G., Delaglio, F. & Bax, A. (1999). Protein backbone angle restraints from searching a database for chemical shift and sequence homology. *J. Biomol. NMR,* **13**, 289-302.

Craven, S. E. & Bredt, D. S. (1998). PDZ proteins organize synaptic signaling pathways. *Cell,* **93**, 495-498.

Craven, S. E., El-Husseini, A. E. & Bredt, D. S. (1999). Synaptic targeting of the postsynaptic density protein PSD-95 mediated by lipid and protein motifs. *Neuron,* **22**, 497-509.

Daniels, D. L., Cohen, A. R., Anderson, J. M. & Brunger, A. T. (1998). Crystal structure of the hCASK PDZ domain reveals the structure basis of class II PDZ domain target recognition. *Nature Struct. Biol.* **5**, 317-325.

Delaglio, F., Grzesiek, S., Vuister, G. W., Zhu, G., Pfeifer, J. & Bax, A. (1995). NMRPipe: a multidimensional spectral processing system based on UNIX pipes. *J. Biomol. NMR,* **6**, 277-293.

Doyle, D. A., Lee, A., Lewis, J., Kim, E., Sheng, M. & MacKinnon, R. (1996). Crystal structures of a complexed and peptide-free membrane protein-binding domain: molecular basis of peptide recognition by PDZ. *Cell,* **85**, 1067-1076.

Farrow, N. A., Muhandiram, R., Singer, A. U., Pascal, S. M., Kay, C. M., Gish, G., Shoelson, S. E., Pawson, T., Forman-Kay, J. D. & Kay, L. E. (1994). Backbone dynamics of a free and phosphopeptide-complexed Src homology 2 domain studied by ^{15}N NMR relaxation. *Biochemistry,* **33**, 5984-6003.

Garrett, D. S., Powers, R., Gronenborn, A. M. & Clore, G. M. (1991). A common sense approach to peak picking in two-, three- and four-dimensional spectra using automatic computer analysis of contour diagrams. *J. Magn. Reson.* **95**, 214-220.

Hillier, B. J., Christopherson, K. S., Prehoda, K. E., Bredt, D. S. & Lim, W. A. (1999). Unexpected modes of PDZ domain scaffolding revealed by structure of nNOS-syntrophin complex. *Science,* **284**, 812-815.

Hsueh, Y. P. & Sheng, M. (1999). Requirement of N-terminal cysteines of PSD-95 for PSD-95 multimerization and ternary complex formation, but not for binding to potassium channel Kv1. 4. *J. Biol. Chem.* **274**, 532-536.

Hsueh, Y. P., Kim, E. & Sheng, M. (1997). Disulfide-linked head-to-head multimerization in the mechanism of ion channel clustering by PSD-95. *Neuron,* **18**, 803-814.

Jaffrey, S. R., Snowman, A. M., Eliasson, M. J., Cohen, N. A. & Snyder, S. H. (1998). CAPON: a protein associated with neuronal nitric oxide synthase that regulates its interactions with PSD95. *Neuron,* **20**, 115-124.

Kay, L. E. & Gardner, K. H. (1997). Solution NMR spectroscopy beyond 25 kDa. *Curr. Opin. Struct. Biol.* **7**, 722-731.

Kim, E., Niethammer, M., Rothschild, A., Jan, Y. N. & Sheng, M. (1995). Clustering of Shaker-type K+ channels by interaction with a family of membrane-associated guanylate kinases. *Nature,* **378**, 85-88.

Kim, E., Cho, K. O., Rothschild, A. & Sheng, M. (1996). Heteromultimerization and NMDA receptor-clustering activity of Chapsyn-110, a member of the PSD-95 family of proteins. *Neuron,* **17**, 103-113.

Kistner, U., Wenzel, B. M., Veh, R. W., Cases-Langhoff, C., Garner, A. M., Appeltauer, U., Voss, B., Gundelfinger, E. D. & Garner, C. C. (1993). SAP90, a rat presynaptic protein related to the product of the *Drosophila* tumoysuppressor gene dlg-A. *J. Biol. Chem.* **268**, 4580-4583.

Koradi, R., Billeter, M. & Wuthrich, K. (1996). MOLMOL: a program for display and analysis of macromolecular structures. *J. Mol. Graph.* **14**, 51-55.

Kornau, H. C., Schenker, L. T., Kennedy, M. B. & Seeburg, P. H. (1995). Domain interaction between NMDA receptor subunits and the postsynaptic density protein PSD-95. *Science,* **269**, 1737-1740.

Kornau, H. C., Seeburg, P. H. & Kennedy, M. B. (1997). Interaction of ion channels and receptors with PDZ domain proteins. *Curr. Opin. Neurobiol.* **7**, 368-373.

Kraulis, P. J. (1991). MOLSCRIPT: a program to produce both detailed and schematic plots of protein structures. *J. Appl. Crystallog.* **24**, 946-950.

Laskwoski, R. A., MacArthur, M. W., Moss, D. S. & Thornton, J. M. (1993). PROCHECK: a program to check the stereochemical quality of protein structures. *J. Appl. Crystallog.* **26**, 283-291.

Lipari, G. & Szabo, A. (1982a). Model-free approach to the interpretation of nuclear magnetic resonance relaxation in macromolecules. 1. Theory and range of validity. *J. Am. Chem. Soc.* **104**, 4546-4559.

Lipari, G. & Szabo, A. (1982b). Model-free approach to the interpretation of nuclear magnetic resonance relaxation in macromolecules. 2. Analysis of experimental results. *J. Am. Chem. Soc.* **104**, 4559-4570.

Lue, R. A., Marfatia, S. M., Branton, D. & Chishti, A. H. (1994). Cloning and characterization of hdlg: the human homologue of the *Drosophila* discs large tumor suppressor binds to protein 4.1. *Proc. Natl Acad. Sci. USA,* **91**, 9818-9822.

Mandel, A. M., Akke, M. & Palmer, A. G., III (1995). Backbone dynamics of *Escherichia coli* ribonuclease HI: correlations with structure and function in an active enzyme. *J. Mol. Biol.* **246**, 144-163.

Maximov, A., Südhof, T. C. & Bezprozvanny, I. (1999). Association of neuronal calcium channels with modular adaptor proteins. *J. Biol. Chem.* **274**, 24453-24456.

McGee, A. W. & Bredt, D. S. (1999). Identification of an intramolecular interaction between the SH3 and guanylate kinase domains of PSD-95. *J. Biol. Chem.* **274**, 17431-17436.

Merritt, E. & Murphy, M. (1994). Raster3D version 2.0: a program for photorealistic molecular graphics. *Acta Crystallog. sect. D,* **50**, 869-873.

Migaud, M., Charlesworth, P., Dempster, M., Webster, L. C., Watabe, A. M., Makhinson, M., He, Y., Ramsay, M. F., Morris, R. G., Morrison, J. H., O'Dell, T. J. & Grant, S. G. (1998). Enhanced long-term potentiation and impaired learning in mice with mutant postsynaptic density-95 protein. *Nature,* **396**, 433-439.

Müller, B. M., Kistner, U., Veh, R. W., Cases-Langhoff, C., Becker, B., Gundelfinger, E. D. & Garner, C. C. (1995). Molecular characterization and spatial distribution of SAP97, a novel presynaptic protein homologous to SAP90 and the *Drosophila* discs-large tumor suppressor protein. *J. Neurosci.* **15**, 2354-2366.

Müller, B. M., Kistner, U., Kindler, S., Chung, W. J., Kuhlendahl, S., Fenster, S. D., Lau, L. F., Veh, R. W., Huganir, R. L., Gundelfinger, E. D. & Garner, C. C. (1996). SAP102, a novel postsynaptic protein that interacts with NMDA receptor complexes *in vivo*. *Neuron,* **17**, 255-265.

Naisbitt, S., Kim, E., Weinberg, R. J., Rao, A., Yang, F. C., Craig, A. M. & Sheng, M. (1997). Characterization of guanylate kinase-associated protein, a postsynaptic density protein at excitatory synapses that interacts directly with postsynaptic density-95/synapse-associated protein 90. *J. Neurosci.* **17**, 5687-5696.

Niethammer, M., Kim, E. & Sheng, M. (1996). Interaction between the C terminus of NMDA receptor subunits and multiple members of the PSD-95 family of membrane-associated guanylate kinases. *J. Neurosci.* **16**, 2157-2163.

Niethammer, M., Valtschanoff, J. G., Kapoor, T. M., Allison, D. W., Weinberg, T. M., Craig, A. M. & Sheng, M. (1998). CRIPT, a novel postsynaptic protein that binds to the third PDZ domain of PSD-95/SAP90. *Neuron,* **20**, 693-707.

Nilges, M., Clore, G. M. & Gronenborn, A. M. (1988). Determination of three-dimensional structures of proteins from interproton distance data by dynamical simulated annealing from a random array of atoms. Circumventing problems associated with folding. *FEBS Letters,* **239**, 129-136.

O'Brien, R. J., Lau, L. F. & Huganir, R. L. (1998). Molecular mechanisms of glutamate receptor clustering at excitatory synapses. *Curr. Opin. Neurobiol.* **8**, 364-369.

Sattler, R., Xiong, Z., Lu, W.-Y., Hafner, M., MacDonald, J. F. & Tymianski, M. (1999). Specific coupling of NMDA receptor activation to nitric oxide neurotoxicity by PSD-95 protein. *Science,* **284**, 1845-1848.

Schepens, J., Cuppen, E., Wieringa, B. & Hendriks, W. (1997). The neuronal nitric oxide synthase PDZ motif binds to -G(D,E)XV* carboxyterminal sequences. *FEBS Letters,* **409**, 53-56.

Schultz, L., Hoffmuller, U., Krause, G., Ashurst, J., Macias, M. J., Schmieder, P., Schneider-Mergener, J.

& Oschkinat, H. (1998). Specific interactions between the syntrophin PDZ domain and voltage-gated sodium channels. *Nature Struct. Biol.* **5**, 19-24.

Sheng, M. (1996). PDZs and receptor/channel clustering: rounding up the latest suspects. *Neuron,* **17**, 575-578.

Songyang, Z., Fanning, A. S., Fu, C., Xu, J., Marfatia, S. M., Chishti, A. H., Crompton, A., Chan, A. C., Anderson, J. M. & Cantley, L. C. (1997). Recognition of unique carboxyl-terminal motifs by distinct PDZ domains. *Science,* **275**, 73-77.

Stein, E. G., Rice, L. M. & Brünger, A. (1997). Torsion-angle molecular dynamic as a new efficient tool for NMR structure calculation. *J. Magn. Reson.* **124**, 154-164.

Stricker, N. L., Christopherson, K. S., Yi, B. A., Schatz, P. J., Raab, R. W., Dawes, G., Bassett, D. E., Jr, Bredt, D. S. & Li, M. (1997). PDZ domain of neuronal nitric oxide synthase recognizes novel C-terminal peptide sequences. *Nature Biotechnol.* **15**, 336-342.

Tochio, H., Ohki, S., Zhang, Q., Li, M. & Zhang, M. (1998). Solution structure of a protein inhibitor of neuronal nitric oxide synthase. *Nature Struct. Biol.* **5**, 965-969.

Tochio, H., Zhang, Q., Mandal, P., Li, M. & Zhang, M. (1999). Solution structure of the extended neuronal nitric oxide synthase PDZ domain complexed with an associated peptide. *Nature Struct. Biol.* **6**, 417-421.

Xia, H., Winokur, S. T., Kuo, W. L., Altherr, M. R. & Bredt, D. S. (1997). Actinin-associated LIM protein: identification of a domain interaction between PDZ and spectrin-like repeat motifs. *J. Cell Biol.* **139**, 507-515.

Zhou, Q., Ruiz-Lozano, P., Martone, M. E. & Chen, J. (1999). Cypher, a striated muscle-restricted PDZ and LIM domain-containing protein, binds to alpha-actinin-2 and protein kinase C. *J. Biol. Chem.* **274**, 19807-19813.

Edited by P. E. Wright

(Received 7 September 1999; received in revised form 2 November 1999; accepted 3 November 1999)